CHAPTER TWELVE

Methods for Studying Mechanical Control of Angiogenesis by the Cytoskeleton and Extracellular Matrix

Akiko Mammoto, Julia E. Sero, Tadanori Mammoto, *and* Donald E. Ingber

Contents

Vascular Biology Program, Departments of Pathology & Surgery, Children's Hospital and Harvard Medical School, Boston, Massachusetts

Methods in Enzymology, Volume 443
ISSN 0076-6879, DOI: 10.1016/S0076-6879(08)02012-0

Abstract

Mechanical forces that capillary endothelial cells generate in their cytoskeleton and exert on their extracellular matrix adhesions feed back to modulate cell sensitivity to soluble angiogenic factors, and thereby control vascular development. Here we describe various genetic, biochemical, and engineering methods that can be used to study, manipulate, and probe this physical mechanism of developmental control. These techniques are useful as *in vitro* angiogenesis models and for analyzing the molecular and biophysical basis of vascular control.

1. Introduction

Most past work on control of angiogenesis focused on the role of soluble angiogenic factors that stimulate capillary endothelial (CE) cell growth and formation of new capillary blood vessels. Although these factors trigger the angiogenic response, cell sensitivity to these soluble cues and resulting vascular development are governed by mechanical forces that cells generate in their cytoskeleton and exert on their extracellular matrix (ECM) adhesions, which feed back to produce changes in cell shape and cytoskeletal structure (Huang and Ingber, 1999; Ingber and Folkman, 1989a; Ingber *et al.*, 1985). Vascular remodeling and directional outgrowth of capillaries also can be influenced by exogenous mechanical stress (e.g., ECM strain because of hemodynamic stresses) *in vitro* as well as *in vivo* (Matsumoto *et al.*, 2007; Pietramaggiori *et al.*, 2007; Tzima, 2006). Thus, there has been great interest in experimental systems that permit analysis of this mechanical form of angiogenic control.

In this chapter, we describe various methods that may be used to control, manipulate, and probe physical interactions between capillary cells and their ECM adhesions, while simultaneously measuring effects on vascular cell behavior and tissue development *in vitro* and *in vivo*. These methods range from use of microfabrication techniques to control the size, shape, and position of cell–ECM contacts to biochemical and genetic methods to manipulate cytoskeletal tension-generation mechanisms that are controlled by small Rho GTPases. Use of these techniques has led to recognition that physical distortion of cell shape and the actin cytoskeleton control cell cycle progression, as well as directional motility in CE cells, and that Rho signaling is critical for angiogenic control *in vitro* and *in vivo*.

2. Control of CE Cell Behavior with Different ECM Coating Densities

More than 20 years ago, we proposed that local variations in physical interactions between cells and their ECM might control the spatial differentials of cell growth and function that drive morphogenesis of tissues, such as branching capillary networks (Huang and Ingber, 1999; Ingber and Folkman, 1989a; Ingber *et al.*, 1985). To explore this hypothesis in the context of angiogenesis, it was necessary to develop methods that would allow us to vary physical interactions between cells and their ECM adhesions in a controlled manner. In early studies, we developed a method to control cell–ECM contact formation by varying the density of ECM molecules coated on otherwise nonadhesive plastic dishes. CE cells spread and proliferated on surfaces with high ECM coating densities, whereas they rounded and failed to grow on low-coating concentrations, even though all cells were stimulated with saturating amounts of soluble angiogenic mitogens (Ingber, 1990; Ingber and Folkman, 1989b; Ingber *et al.*, 1987). Importantly, when CE cells were cultured at a high density on a moderate coating density that only partially resisted cell traction forces, these cells collectively retracted and differentiated into branching capillary networks lined by hollow endothelial-lined tubular structures (Fig. 12.1) (Ingber and Folkman, 1989b). Moreover, the importance of mechanics for this form of differentiation control was shown by the fact that tube formation also could be induced on the highest ECM density that normally promotes cell growth by increasing the cell plating density and, thereby, increasing cumulative cell traction forces (Fig. 12.1). This same technique was shown to be useful for control of growth and differentiation of other cell types, including primary hepatocytes (Mooney *et al.*, 1992) and vascular smooth muscle cells (Kim *et al.*, 1998; 1999; Lee *et al.*, 1998). In fact, this is a popular technique, because it provides a method to exert fine control over cell shape

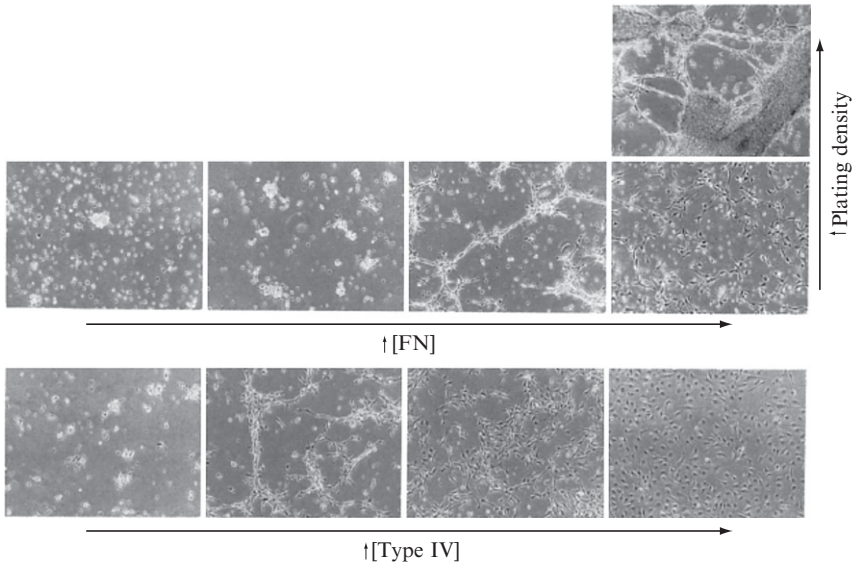

Figure 12.1 Control of angiogenesis *in vitro* by modulating ECM coating density. Bacteriologic dishes were precoated with 10, 50, 100, or 2500 ng/cm^2 (from left to right) of FN or type IV collagen (type IV). The highest concentration shown was saturating for both CE cell attachment and spreading. These phase-contrast views show that cell attachment and spreading increase in parallel with the number of ECM molecules available for cell attachment. Tube formation was only observed on dishes of intermediate adhesivity when cells were plated at a moderate density (4×10^4 cells/cm^2). CE cells formed extensive capillary networks on the highest FN coating density when higher numbers were plated (2×10^5 cells/cm^2; top right). Tube formation was observed on lower coating densities on type IV than on FN; type IV promoted more extensive cell attachment and spreading at all coating concentrations (original magnification of 50×; reprinted with permission from Ingber and Folkman, 1989b).

and function with commercially available substrates and ECM molecules that can be accomplished in any laboratory around the world.

2.1. Cell culture

CE cells isolated from bovine adrenal cortex (Folkman *et al.*, 1979) are maintained for 10 to 15 passages on gelatin-coated tissue culture dishes in low-glucose Dulbecco's modified Eagles medium (DMEM; Invitrogen) supplemented with 10% fetal calf serum (FCS) (Hyclone), 10 m*M* HEPES (JRH-Biosciences), and L-glutamine (0.292 mg/ml), penicillin (100 U/ml), streptomycin (100 μg/ml) at 37° under 10% CO_2 (Chen *et al.*, 1997; Ingber, 1990; Ingber and Folkman, 1989b; Matthews *et al.*, 2006; Numaguchi *et al.*, 2003).

2.2. Matrix coating procedures

To control cell–ECM contact formation, bacteriologic plastic substrates (35-mm petri dishes; Falcon, Lincoln Park, NJ) or multichamber glass culture slides (Lab-Tek; Miles) are precoated with fibronectin (FN; Cappel Laboratories, Malvern, PA) or type IV collagen (Calbiochem, San Diego, CA) at various densities (22 ng/cm^2 to 666 ng/cm^2) with a carbonate buffer-coating technique (Huang *et al.*, 1998; Ingber, 1990; Ingber *et al.*, 1987; Mammoto *et al.*, 2004). Various amounts of human serum FN and collagen IV are dissolved in 0.1 *M* carbonate buffer (pH 9.4) and allowed to adsorb for 24 h at 4°. Dishes are washed with phosphate-buffered saline (PBS), DMEM, and blocked with 1% bovine serum albumin (BSA, Fraction V; Intergen, Purchase, NY) in DMEM for 1 h at 37° before use. CE cells are plated on the coated dishes in DMEM supplemented with 5 μg/ml transferrin (Collaborative Research, Lexington, MA), 10 μg/ml high-density lipoprotein (specific gravity, 1.063 to 1.21 g/cm^3; Perimmune, Rockville, MD), and 2 ng/ml recombinant basic FGF (Takeda Chemical Industries, Osaka, Japan). BSA (10 mg/ml) is also included as colloid in some studies without altering our results.

2.3. Analytical methods

CE cells are plated in defined medium on the ECM-coated substrates at a moderate (2 to 5 $\times$ 10^4 cells/cm^2) density and cultured for hours to days to analyze the effects on cell adhesion, spreading, cytoskeletal organization, growth, and differentiation with time-lapse cinematography, electron microscopic analysis, and measurement of DNA synthesis with [^{3}H] thymidine (Ingber and Folkman, 1989b). Extensive branching capillary networks consistently form within 24 to 48 h when CE cells are plated on dishes of intermediate adhesivity (100 to 500 ng FN or type IV collagen/cm^2), although tube formation also can be induced on higher ECM densities (>2500 ng FN or type IV collagen/cm^2) by plating cells at a higher density (1 to 3 $\times$ 10^5 cells/ cm^2) (Fig. 12.1) (Ingber and Folkman, 1989b). Phase-contrast images of living cells are recorded with in inverted microscope (Diaphot; Nikon Inc., Garden City, NY) with film (Plus-X-pan; Eastman Kodak Co., Rochester, NY). For electron microscopic analysis, reorganized capillary tube are fixed in 2.5% glutaraldehyde/ 2% paraformaldehyde in 0.1 *M* sodium cacodylate buffer, pH7.4, post-fixed in 1% osmium tetroxide, dehydrated in a graded series of alcohols, and embedded in Epon. Thin sections (800 A thick) are cut on an UltraCut microtome (Reicher Scientific Instruments, Buffalo, NY), counterstained with uranyl acetate and lead citrate, and studied under an electron microscope (No. 100B; JOEL USA, Cranford, NJ). To measure of DNA synthesis, light microscopic autoradiography is carried out by adding [^{3}H] thymidine

(1 mCi/ml final concentration; New England Nuclear, Boston, MA) to the defined medium during the first 24 h of culture (Ingber, 1990; Ingber and Folkman, 1989b). Radiolabelled CE cells are fixed with Karnovsky's solution, dehydrated with methanol, and overlaid with nuclear track emulsion (NTB-2; Eastman Kodak Co.). Autoradiographic grains are developed with D-19 developer (Eastman Kodak Co.).

3. Control of CE Cell Fate Switching by Use of Microfabricated ECM Islands

Although the ECM coating-density method for cell shape control is powerful, it may be complicated by the fact that altering ECM-coating densities also may change the degree of integrin receptor clustering on the cell surface, which can alter intracellular biochemical signaling responses independent of cell shape (Schwartz *et al.*, 1991). We, therefore, developed another technique that permits one to vary cell shape and cytoskeletal distortion while maintaining the ECM coating density and concentration of soluble angiogenic factors constant. This approach involved use of a microcontact printing technique (Kumar and Whitesides, 1994; Prime and Whitesides, 1991) to microfabricate ECM islands of defined size, shape, and position on the micrometer scale that are the same size as individual cultured cells, surrounded by nonadhesive barrier regions (Fig. 12.2A) (Chen *et al.*, 1997; Singhvi *et al.*, 1994). By use of this method, we showed that single adherent, growth factor–stimulated CE cells increase their ability to pass through the G1/S transition and proliferate when they are cultured on large ECM islands (>2500 μm^2) that promote cell spreading, whereas cells turn off growth and become quiescent on intermediate sized islands (1000 to 2000 μm^2); the same CE cells switch on apoptosis (programmed cell death) when spreading is completely inhibited by plating cells on tiny (<500 μm^2) islands (Chen *et al.*, 1997). Furthermore, when CE cells are cultured on long thin (10 to 30 μm) ECM islands in the same growth factor–containing medium, they differentiate into linear hollow capillary tubes (Dike *et al.*, 1999). The same micropatterned ECM substrates have been shown to exert similar control over cell fate switching in many other kinds of cells as well, including vascular smooth muscle cells, hepatocytes, and fibroblasts (Chen *et al.*, 2000; Dike *et al.*, 1999; Thakar *et al.*, 2003).

Directional cell motility is critical for normal tissue development and the immune response, angiogenesis, and cancer metastasis. Most work on directional control of cell movement has focused on gradients of soluble chemokines (Ridley *et al.*, 2003) that, in turn, generate intracellular gradients of signal transduction (Ridley *et al.*, 2003; Van Haastert and Devreotes, 2004). However, cell movement also can be influenced by physical

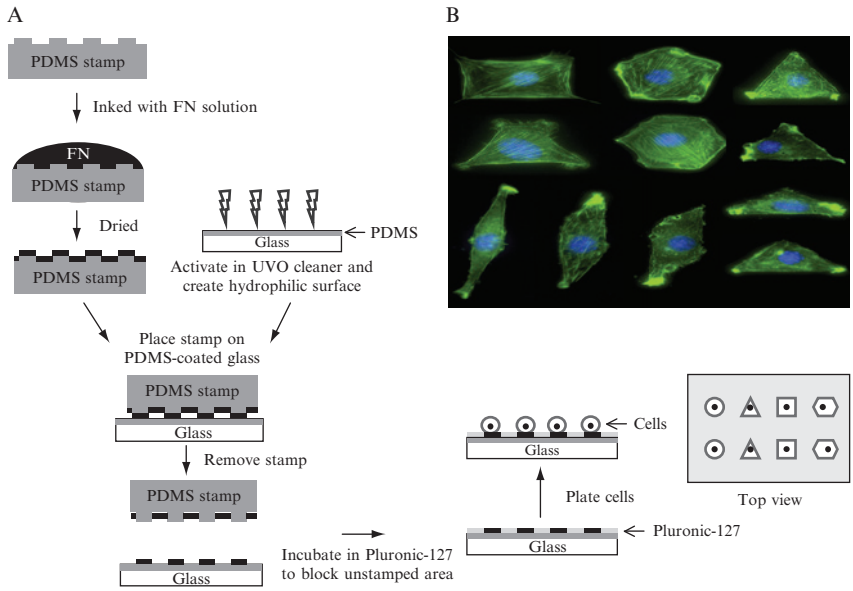

Figure 12.2 Method for controlling cell shape and function with micrometer-scale ECM islands microfabricated with microcontact printing. (A) Schematic of microcontact printing technique with soft lithography and direct printing of protein onto the surface of a thick layer of PDMS. See text for a detailed description. (B) Fluorescence microscopic images of CE cells cultured on microscale FN islands (900 μm^2) of different geometric shapes and stained with fluorescent-phalloidin to visualize F-actin and DAPI to visualize nuclei. Note that cells preferentially extend new cell processes from their corners and that they prefer acute rather than obtuse angles.

interactions between cells and their ECM adhesions. For example, cells move from regions of high ECM compliance to more stiff regions, a process as known as "durotaxis" (Discher *et al.*, 2005; Lo *et al.*, 2000). As described previously, when plated on single-cell–sized ECM islands of different geometric shapes created with microfabrication techniques, various cells preferentially extend new motile processes (e.g., lamellipodia, filopodia, microspikes) from their corners rather than along their edges (Brock *et al.*, 2003; Parker *et al.*, 2002). Focal adhesions are also preferentially formed in their corners near sites where new lamellipodia will form when cells are stimulated with soluble chemokines, and cells on circular islands (i.e., without corners) do not exhibit any directional bias (Parker *et al.*, 2002).

Importantly, this microcontact printing technique also can be used to study directional cell motility. CE cells, fibroblasts, and muscle cells cultured on angulated polygonal ECM islands (e.g., squares, rectangles, hexagons, pentagons) preferentially extend new motile processes, including lamellipodia, filopodia, and microspikes, from the corners of these islands (Fig. 12.2B), whereas cells display no directional bias when they are

cultured on circular ECM islands (Brock *et al.*, 2003; Parker *et al.*, 2002). These cells preferentially exert greatest traction force, form focal adhesions, and deposit new ECM fibrils in their corners, and thus this technique is especially well suited for studying spatial control of motility signaling and oriented lamellipodia formation in adherent cells.

Microcontact printing also can be used to engineer substrates containing microarrays of much smaller (1 to 8 μm diameter) ECM islands that are on the same scale as individual focal adhesions (Fig. 12.3A) (Chen *et al.*, 2003; Tan *et al.*, 2003). Because focal adhesions seem to preferentially form directly behind the leading edge of cells migrating in the direction of increasing ECM stiffness (Beningo *et al.*, 2001; Pelham and Wang, 1997) and changes in mechanical force transfer across integrins can modulate focal

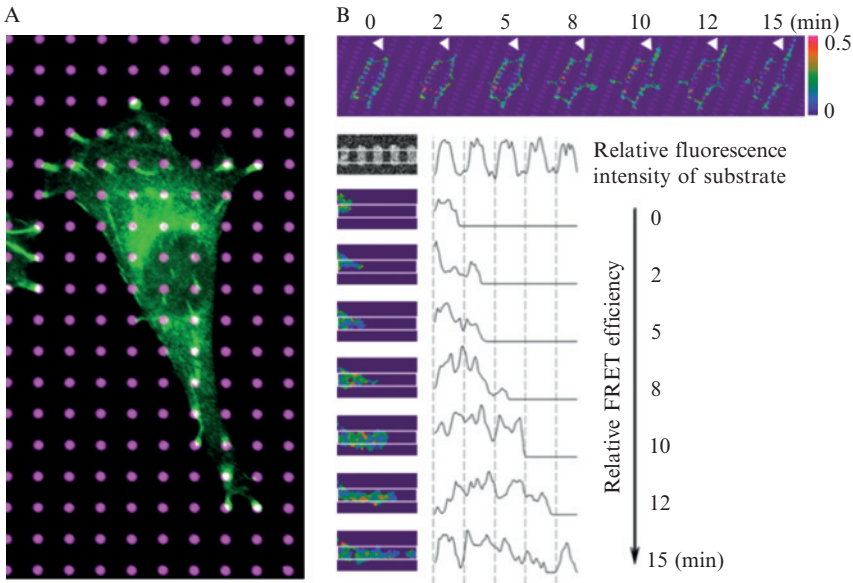

Figure 12.3 Method for analyzing spatial control of motility signaling pathways by cell–ECM interactions. (A) Immunofluorescence microscopic image of a cell cultured for 8 h on microarrays of circular 1-μm diameter rhodamine-FN–coated islands spaced 3 μm from neighbors and stained with anti-vinculin antibodies; white indicates formation of focal adhesions directly above the ECM islands. (B) Rac-FRET analysis of a cell spreading over an array of multiple FN islands (1 × 3 μm). *Upper;* Low-magnification view showing the same cell during a 15-min period of spreading showing increased Rac activity (relative FRET efficiency shown in color bar at right) concentrated in FAs directly above periphery FN islands. *Lower;* Higher power view of 5 FN islands showing the leading edge of the cell moving progressively from FN island to island (left to right) and activating Rac activity locally within minutes after forming an adhesive contact (FA) with the new ECM substrate (black line indicates relative FRET efficiency).

adhesion assembly (Riveline *et al.*, 2001), the spatial positioning of focal adhesions may determine the location in which new motile processes form and, hence, govern the direction in which cells move. Recently, we used microarrays of focal adhesion–sized ECM islands created with this microcontact printing method to demonstrate that we can influence the direction of cell spreading and movement over a period of multiple hours by altering focal adhesion shape or position (Xia *et al.*, 2008). These findings are physiologically important, because cells also preferentially extend and migrate along ECMs with specialized shapes (e.g., fibrils) during tissue development (Nakatsuji and Johnson, 1984) and tumor angiogenesis (Folkman *et al.*, 1989). Again, this method may be useful for any adherent cell type that exhibits directional movement.

3.1. Cell culture

These studies are carried out with bovine CE cells cultured as described previously; with primary human pulmonary CE cells (Lonza Inc.) cultured for 3 to 5 passages in EBM medium (Lonza) supplemented with 10 ng/ml human recombinant epidermal growth factor (EGF), 12 mg/ml bovine brain extract, 1 mg/ml hydrocortisone, and 10% FBS at 37° under 5 % CO_2; or with NIH 3T3 cells cultured in DMEM/F12 nutrient media containing 10% bovine calf serum, 2 m*M* glutamine, penicillin (100 U/ml), streptomycin (100 mg/ml), 250 mg/ml amphotericin B, and 205 mg/ml of sodium deoxycholate (Life Technologies) under 5% CO_2 (Yu *et al.*, 2001).

3.2. Microcontact printing

Micropatterning techniques include four main categories of techniques: photolithography (Bhatia *et al.*, 1993), soft lithography (Whitesides, *et al.*, 2001), direct writing (Odde and Ren, 1999; Roth, *et al.*, 2004; Veiseh, *et al.*, 2004), and laser patterning (Corey, *et al.*, 1991; Duncan, *et al.*, 2002; Vaidya, *et al.*, 1998). Among them, soft lithography has drawn the largest attention and found the most extensive applications. We mainly use two methods of microcontact printing to study shape regulation of cell behavior that involved use of either self-assembled monolayers (SAMs) of alkane thiols on gold-plated substrates (Chen *et al.*, 1997; Dike *et al.*, 1999; Parker *et al.*, 2002; Singhvi *et al.*, 1994) or micropatterning proteins directly on poly (dimethyl-siloxane) (PDMS) (Lele *et al.*, 2007; Xia *et al.*, 2008) (Fig. 12.2A).

In both methods, the desired pattern of ECM islands is designed with computer software (e.g., AutoCAD) and transferred to a mask with high-resolution laser printing or by electron-beam etching of chromium on glass (for smaller features). PDMS stamps are fabricated by casting the polymer onto silicon wafers that have been etched by photolithography with micro-scale features (see Whitesides [2001] for more details). To micropattern

SAMs on substrates sputter-coated with a thin (12-nm) layer of gold, the PDMS stamp is inked with an ethanol solution of hexadecanethiol, dried thoroughly with filtered air or nitrogen, and then gently brought into conformal contact with the gold substrate, such that only the raised features of the stamp make contact for at least 30 sec. This prints the gold with SAMs that will allow protein adsorption; the remainder of the substrate is blocked by incubating in a solution of $(EG)_3OH$-terminated alkane thiols, forming SAMs that will resist protein and cell adsorption. Finally, the substrates are rinsed and incubated with ECM proteins, such as FN, type IV collagen, or laminin, which adsorbs exclusively to the printed areas. After washing off excess protein, taking care not to allow the substrates to dry out, the microcontact printed surface is ready for cell plating. Even in the presence of serum, cells will adhere only to the printed, adhesive areas. We have published details methods for this technique previously (Chen *et al.*, 2000).

More recently, we have used a more simple, cost-effective method of microcontact printing that allows direct stamping of protein onto the surface of a thin layer of PDMS (Sylgard-184, Dow Corning) (Tan *et al.*, 2002) (Fig. 12.2A). We typically use a 9:1 ratio of elastomer base to curing agent, which forms a moderately stiff substrate (Young's modulus greater than 1 MPa) when cured (Gray *et al.*, 2003). The base and curing agent should be well mixed and degassed before use with a vacuum or quick spin (1 to 2 min) at 1000 rpm in a tabletop centrifuge. Coverslips are coated with a spin coater: a drop of PDMS (200 μl for a 25-mm $\times$ 25-mm coverslip, Corning) is applied to the center of the coverslip and spun at 4000 rpm for 4 min. The polymer can be cured by incubation at 60° for 1 h or at room temperature for at least 24 h. Coated coverslips can then be cut with a diamond pen to desired size. The resulting layer of PDMS is only tens of microns thick and optically clear, allowing high magnification imaging of cells through the coated coverslip. Coverslip-bottomed petri dishes (MatTek) can be spin-coated in the same manner to perform high-magnification imaging of live cells on microcontact printed substrates.

The PDMS stamps are cleaned in 70% ethanol in a sonicating water bath for 30 min, rinsed with water, and dried with filtered compressed air or nitrogen gas. The surface of the clean stamps containing the raised micropatterned features are incubated with 50 μg/mL FN (or other ECM protein) in aqueous solution for 1 h and dried thoroughly with filtered nitrogen gas or compressed air. To ink the hydrophobic stamps, it is helpful to "paint" the protein solution onto the patterned surface with a pipet tip. Before stamping, the hydrophilic PDMS-coated coverslips are made hydrophilic by treatment with plasma, which causes the surface to become temporarily negatively charged and adsorptive for proteins (Whitesides *et al.*, 2001). We plasma treat the PDMS-coated coverslips in a Jelight UVO cleaner (Specialty Coating Systems G3P-8, Cookson Electronics) for 8 min, while the inked PDMS stamps are rinsed in water or PBS and

dried. The stamps are pressed gently against the plasma-treated PDMS surface with the fingertips or forceps within 15 min of plasma treatment to ensure complete contact of stamp with substrate. By use of rhodamine-conjugated fibronectin (Cytoskeleton, Denver, CO), we have found that 1 to 3 min of contact is sufficient to efficiently transfer protein to the PDMS-coated coverslip, but less than 30 sec contact may result in incomplete protein transfer. Unstamped areas are then made nonadhesive by incubating the substrates in 1% Pluronic 127 in PBS for 1 h at room temperature or overnight at 4°. Pluronic surfactants are nontoxic triblock polymers whose polypropylene segments adsorb to the hydrophobic PDMS surface, whereas their polyethylene glycol segments block protein adsorption (Amiji and Park, 1992; Chen *et al.*, 2004). Before use, substrates are washed three times with PBS. Microstamped PDMS substrates should be used within a few days of preparation, and they are most useful for short-term experiments (less than 1 week).

3.3. Cell culture on microfabricated ECM islands

Cells that are grown to confluence in serum-containing medium (Chen *et al.*, 1997; Huang *et al.*, 1998; Yu *et al.*, 2001) are serum-deprived for 1 to 2 days before use in experiments. These quiescent cells are then trypsinized and plated sparsely (3×10^3 cells/cm^2) on the micropatterned ECM substrates to ensure that individual islands are seeded with single cells. For morphologic and cell cycle analysis, bovine CE cells are cultured in serum-free DMEM supplemented with bFGF (5 ng/ml) and primary human pulmonary CE cells are cultured with EGM2 supplemented with 2% FBS, 10 μg/ml high-density lipoprotein and 5 μg/ml; transferring for 18 to 24 h. When bovine CE and NIH3T3 cells are cultured for extended times (up to 30 min) on the microscope stage, these studies are carried out in bicarbonate-free minimum essential medium (MEM) containing Hank's balanced salts lacking phenol red and bicarbonate (Sigma Chemical Co., St. Louis, MO), MEM amino acids (Sigma), MEM vitamins (Sigma), 2 m*M* L-glutamine, 1 m*M* sodium pyruvate, 20 m*M* *N*-2-hydroxyethylpiperazine-N#-2-ethanesulfonic acid, D-glucose (1 g/L), hydrocortisone (1 μg/ml), and 1% BSA. This medium is supplemented with 20 μg/ml high-density lipoprotein and 5 μg/ml transferrin for studies with endothelial cells; studies with fibroblasts used the same medium with high glucose (5 g/L).

3.4. Analysis of cell cycle progression

For cell cycle analysis, human CE cells are synchronized by treatment with 40 m*M* lovastatin (Merck, Rahway, NJ) in standard culture medium for 32 h (Huang *et al.*, 1998) or serum deprivation for 48 h (Mammoto *et al.*, 2004). The cells are trypsinized, washed, and replated on the micropatterned

islands in culture medium described previously. The ability of cells to enter S phase is measured by quantitating the percentage of cells that exhibited nuclear incorporation of 5-bromo-29-deoxyuridine (BrdU), as detected with a commercial assay (Amersham, Arlington Heights, IL). Cells are fixed in 5% acetic acid/90% ethanol for 30 min at room temperature. BrdU-positive cells are identified by incubating cells with anti-BrdU antibody and nuclease (RPN202, Amersham Biosciences) for 60 min and stained with biotinylated anti-mouse Ig antibodies and Texas red avidin (Vector Laboratories, Burlingame, California). BrdU-positive cells are visualized and scored with a Nikon epifluorescence microscope with 20× objectives; all nuclei are counterstained with DNA binding dye, 4,6-diamino-2-phenylindole (DAPI; 1 μg/ml). At least 12 random fields with a total of 500 cells are counted per sample (Huang *et al.*, 1998; Numaguchi *et al.*, 2003).

The extent of pRb hyperphosphorylation is also a marker of G1/S transition, which is measured indirectly with an *in situ* nuclear labeling technique (Huang *et al.*, 1998; Latham *et al.*, 1996; Mittnacht and Weinberg, 1991). This *in situ* technique is based on the finding that hyperphosphorylated pRb easily dissociates from nuclei when treated with a nuclear extraction buffer (Mittnacht and Weinberg, 1991). Cells are washed once in PBS after 18 h of culture, incubated in nuclear extraction buffer (10 m*M* HEPES-KOH, pH 7.9, 10 m*M* KCl, 1.5 m*M* $MgCl_2$, 0.1% Triton X-100, 1 m*M* dithiothreitol) for 15 min at room temperature, fixed for 20 min in 4% PFA/PBS, and washed with 0.1% BSA/PBS. pRb is visualized by indirect immunostaining with anti-human pRb antibody LM95.1 (2 g/ml; Calbiochem); cells are also counterstained with DAPI to facilitate quantitation of the percentage of pRb-negative nuclei. Negative pRb staining indicates cells that contain hyperphosphorylated pRb that dissociated from nuclear matrix and, hence, cells that successfully passed through the late G1 restriction point (Huang *et al.*, 1998; Latham *et al.*, 1996; Mittnacht and Weinberg, 1991).

3.5. Analysis of directional lamellipodia extension

For studies on directional extension of new motile processes on single cell–sized ECM islands, lamellipodia formation is synchronously activated in NIH 3T3s by addition of human PDGF-BB (5 ng/mL, BioVision, Mountain View, CA) and in bovine CE cells by addition of bFGF (5 ng/mL) or 10% calf serum. Living cells are visualized with a Hamamatsu CCD camera on a Nikon Diaphot 300 inverted microscope equipped with phase-contrast optics and epifluorescence illumination. Temperature is controlled by a stage mount (Micro Video Instruments, Avon, MA) equipped with a temperature controller (Omega technologies Co., Stamford, CT). The total projected area of lamellipodia per cell is quantitated with the

computerized image acquisition and analysis tools of IP Lab Spectrum and RatioPlus software (Scanalytics, Fairfax, VA). F-actin, vinculin, fibronectin, and DNA (nuclei) are visualized in cells fixed with 4% PFA with phalloidin (300 ng/ml), mouse anti-vinculin antibody, rabbit anti-fibronectin antibody, and DAPI staining (all from Sigma), respectively (Parker *et al.*, 2002) (Fig. 12.2B). We have found that 40 × 40 μm and 30 × 30 μm square ECM islands are highly effective for this analysis in bovine CE cells and NIH3T3 fibroblasts, respectively. However, any shape and size island can be used for these experiments, and the optimal island geometry needs to be empirically determined for each cell type and set of experimental conditions.

Any cell projection that extends over the nonadhesive region surrounding the ECM island and stains positively for F-actin is considered a lamellipodium. But to account for registration errors, we only count projections that are greater than 1 μm^2 in area and have a pixel intensity greater than background. To determine relative changes in lamellipodia length in different regions of the cell, corners are defined as parts of the square perimeter within 6 μm from the intersection of the two sides; sides are defined as the 18-μm interval between these corner regions. To control for bias in morphometric calculations because of the geometry of the orthogonal corner regions relative to the linear sides and the large range of lamellipodia morphology, the normalized lamellipodia length is determined by transforming the total lamellipodia area measured in each region into a similar shaped region (corner or side) composed of a lamellipodium that extended equally from all points along its perimeter. Total cumulative data may be presented by overlaying 20 to 40 images of cells cultured on FN islands and stained for F-actin with fluoresceinated-phalloidin. The pixel occupancy at each position relative to the FN island is determined with IP Lab software, and the pixel distribution is color coded for frequency. Immunofluorescence microscopy is carried out with the epifluorescence optics of the Nikon Diaphot microscope.

3.6. Microcontact printing of microarrays of focal adhesions sized ECM islands

Various different planar microarrays of focal adhesion-sized circular or linear FN islands, separated by nonadhesive regions, are created by use of microcontact printing (Chen *et al.*, 2003; Tan *et al.*, 2003; Xia *et al.*, 2008). As displayed in Fig. 12.3, these include patterns of 1-μm diameter circular FN islands that are either separated by 3 μm in both the X and Y directions (1C-3,3) or by 1.5 μm in the X direction and 3 μm in the Y direction (1C-1.5,3); linear FN islands 1 μm high (Y direction) and 3 or 8 μm wide (X direction) separated by 3 μm in both directions (3L-3,3 and 8L-3,3 respectively); linear FN islands 3 μm wide × 1 μm high separated by 4.5 and 1 μm in

X and Y directions, respectively (3L-4.5,1); and linear 8 μm wide $\times$ 1 μm high FN lines equally spaced by 3 μm in both directions, but staggered along a 60-degree offset (8L-3,3st). Subconfluent NIH 3T3 cell monolayers are serum-starved for 1 day, trypsinized, and plated on micropatterned substrates in DMEM containing high-density lipoprotein (10 μg/ml;), transferrin (5 μg/ml;), and 1% BSA. The plating density is low to minimize cell–cell contacts.

3.7. Morphometric analysis of cell spreading, orientation, and directional movement

Live cell images are carried out as described previously (Brock *et al.*, 2003; Parker *et al.*, 2002), and fluorescence images are acquired on a Leica TCS SP2 confocal laser scanning microscope with a 63 $\times$ /1.4 NA oil immersion objective and processed with Leica software or Adobe Photoshop. Morphometric analysis of cell shape, orientation, and migration is carried out by outlining the borders of individual cells within differential interference contract images with the computerized image acquisition and analysis tools described previously; 25 to 50 cells are analyzed for each experimental condition. Cell elongation is defined as the ratio of the maximal to minimal cell length. In the migration assays, cells are stimulated with PDGF-BB (50 ng/ml) and the centroids of the migrating cell recorded at 20-min intervals over 8 h are plotted and connected to generate the migration path, which is then used to calculate the speed and direction of cell migration.

Cell movement is analyzed by its speed, direction, and pattern of the migration path. For example, cell migration direction is random (45 degrees with a wide distribution) on the isotropic FN circles and more oriented on the anisotropic patterns and linear FN islands. Importantly, even cells migrated in a random Brownian walk on the isotropic array of FN circles, cells could be made to preferentially migrate in either the X or Y direction with great efficiency by decreasing interisland spacing in the X or Y direction with the 1C-1.5, 3 and 3L-4.5,1 substrates, respectively.

4. Control of Cell Fate Switching by Modulating the Cytoskeleton

Cell fate switching also can be controlled in CE cells by altering cytoskeletal structure from within. For example, CE cell growth can be inhibited by treating cells with pharmacologic agents that disrupt the actin cytoskeleton, such as cytochalasin D (Cyto D) or latrunculin B (LatB), or with drugs that inhibit cytoskeletal tension generation (e.g., 2,3-butanedione 2-monoxime; BDM) (Huang *et al.*, 1998; Mammoto *et al.*, 2004).

Treatment of cells with Cyto D or with nocodazole (Noc) to depolymerize the microtubule system also promotes apoptosis in these cells (Flusberg *et al.*, 2001). Alternately, overexpression of nonmuscle caldesmon (CaD), a protein component of the contractile actomyosin filament apparatus, which binds to actin, myosin, tropomyosin, and calmodulin (Huber, 1997; Matsumura and Yamashiro, 1993), can be used to disrupt actin stress fibers, disassemble focal adhesions, and induce cell retraction in cultured cells (Helfman *et al.*, 1999; Numaguchi *et al.*, 2003). When CaD binds to actin, it inhibits the ATPase activity of actomyosin in a calcium- and calmodulin-dependent manner (Chalovich *et al.*, 1998; Marston *et al.*, 1994) and thereby suppresses formation of actin fiber bundles and focal adhesions (Helfman *et al.*, 1999). We used an adenovirus-mediated expression system under control of a tetracycline (Tet)-inducer (AdTet-Off) to achieve efficient, synchronous, and tunable expression of CaD-GFP in CE cells and found that it is involved in angiogenesis (Numaguchi *et al.*, 2003).

4.1. Pharmacologic modifiers of cytoskeletal structure

To disrupt actin microfilaments and microtubules, cells are incubated with Cyto D (1 μg/ml; Sigma), Lat B (0.1 μg/ml; Calbiochem, La Jolla, CA) or Noc (10 μg/ml; Sigma) for 15 min before cells are plated on ECM-coated substrates in the continued presence of the drugs. These doses have been shown to fully disrupt the integrity of actin microfilaments and microtubules in CE cells (Flusberg *et al.*, 2001; Huang *et al.*, 1998; Ingber *et al.*, 1995; Mammoto *et al.*, 2004). To inhibit cytoskeletal tension generation and prevent the formation of focal adhesion and actin bundles in CE cells, cells are treated with 5 m*M* BDM (Sigma), a dose that does not significantly alter intracellular calcium concentration (Blanchard *et al.*, 1990; Chicurel *et al.*, 1998; Chrzanowska-Wodnicka and Burridge, 1996). The specificity of these cytoskeletal-disrupting agents in CE cells has been demonstrated experimentally (Ingber *et al.*, 1995; Wang *et al.*, 1993).

4.2. Control of cell shape and function with adenoviral CaD

To create an adenoviral form of CaD, the plasmid containing GFP-tagged cDNA encoding the full-length rat nonmuscle CaD gene (kindly supplied by Dr David M. Helfman, Cold Spring Harbor Laboratory) is used as the template plasmid. The shuttle vector plasmid pTRE2-shuttle containing the minimal cytomegalovirus promoter and tet-operator sequences cloned upstream of the cDNA to be expressed and the Tet-Off system is purchased from BD Biosciences Clontech (Palo Alto, CA). The GFP-CaD gene is excised from the template plasmid at *XbaI*/*BamHI* sites, and both intruding ends are blunted with a DNA blunting kit (TAKARA, Japan) and ligated at the *EcoRV* site of the pTRE2-shuttle vector. Human kidney–derived 293

epithelial cells (QBIOgene, Carlsbad, CA) are cultured in 10% FBS/DMEM to a subconfluent density before transfection. The pTRE2 shuttle vector containing GFP-CaD gene is ligated with the adenoviral genome DNA (Clontech) and transfected into the 293 cells diluted in Optimem (Invitrogen, Carlsbad, CA) with transfection reagent, Lipofectamine 2000 (Invitrogen). After 2 or 3 days, cells that become round and detach from the substrate because of the cytopathic effect of the adenoviral infection float in the medium until 7 days after transfection. The cells are then collected in a tube, repeatedly frozen, thawed five times, and collected by centrifugation (1500 rpm). The supernatants containing recombinant adenovirus particles encoding GFP-CaD (AdGFP-CaD; first seed) are aliquoted and stored at −80°. To obtain higher titers of the adenoviral vectors, this process is repeated two additional times. The final (third) round produces viral titers ranging from 10^9 to 10^{10} pfu/ml, as determined by plaque assay in 293 cells. Induction of expression of the integrated target gene is controlled solely by removing Tet from the culture medium. The presence of the cDNA insert is confirmed by direct observation of disruption of actin fibers in GFP-labeled cells transduced with AdGFP-CaD and AdTet-Off in Tet-free medium and by Western blot analysis of cell lysates.

To determine the effects of expressing AdGFP-CaD, 1 day after bovine CE cells are plated, the DMEM/10%FBS is replaced 0.4% FBS/DMEM containing 10^8 pfu/ml of AdGFP-CaD, AdTet-Off, and 10 μg/ml of Tet, and cells are cultured for 36 to 48 additional hours (Numaguchi *et al.*, 2003). After CE cells synchronize in G0 by culturing in low serum for 2 to 3 days, GFP-CaD expression is induced by culturing the cells in the same low-serum medium without Tet for 24 additional hours. Then, cells are induced to reenter into the cell cycle by replacing the medium with 10% FBS/DMEM containing BrdU, in the continued absence of Tet. Control cultures are treated identically except in the medium with Tet throughout the entire experiment. Progression of quiescent CE cells through the cell cycle and into S phase is measured with BrdU analysis as described previously (Huang *et al.*, 1998; Numaguchi *et al.*, 2003).

To measure effects on apoptosis under similar conditions, CE cells cultured for 24 h under various level of induction of GFP-CaD are fixed with 4% PFA/ PBS for 15 min at room temperature. The fixed cells are permeabilized with 0.1% sodium citrate/0.1% Triton-X 100 in PBS and stained with terminal deoxynucleotidyl transferase dUTP nick end labeling (TUNEL) enzyme reagent (*In situ* Cell Death Detection kit; Roche Molecular Biochemicals, Indianapolis, IN). The apoptosis index is calculated as the percentage of DAPI-labeled nuclei that exhibit positive TUNEL staining as detected with fluorescence microscopy (Flusberg *et al.*, 2001; Huang *et al.*, 1998; Numaguchi *et al.*, 2003).

We also use a caspase assay as another way to detect apoptosis (Flusberg *et al.*, 2001). Caspase proteases play an essential role in apoptosis by

degrading specific structural, regulatory, and DNA repair proteins within a cell (Casciola-Rosen *et al.*, 1994; Lazebnik *et al.*, 1994). Caspase-9 and -8 are activated early in the apoptotic cascade, which is released from the mitochondria in response to apoptotic stimuli (Li *et al.*, 1997). Activated caspase then initiates the proteolytic activity of other downstream caspases, including caspase-3 and others (Muzio *et al.*, 1997; Srinivasula *et al.*, 1996). For caspase activity analysis, the cells are lysed in ice-cold lysis buffer (ApoAlert Fluorometric Caspase-3 Activity Assay; Clontech, Palo Alto, CA), centrifuged, and the supernatants are transferred to a 96-well plate. Lysates are incubated for 1 h at 37° with the caspase-3–specific fluorescent substrate DEVD-AFC (50 μM; CLONTECH) or the caspase-8–specific substrate IETD-AFC, and fluorescence is measured with the use of a fluorometric plate reader (Bio-Rad, Hercules, CA) at 380-nm excitation and 460-nm emission. For caspase inhibition, cell monolayers are pretreated with the caspase inhibitor z-VAD.fmk (100 μM; Calbiochem, San Diego, CA) for 1 h at 37° before the start of the experiment and after replating.

5. Analysis of the Mechanism of Cell Shape–Dependent Growth Control

Adhesion-dependent control of cell growth requires joint regulation of the ERK/MAPK pathway by integrins and growth-factor receptors during G1-phase of the cell cycle (Meloche *et al.*, 1992; Weber *et al.*, 1997; Zhu and Assoian, 1995). However, activation of ERK/MAPK is not sufficient for passage through the late-G1 checkpoint. For example, when CE cells are prevented from spreading by culturing them in the presence of soluble mitogens on dishes coated with a low density of FN or on small, micrometer-sized, high-density FN islands as described previously, the G1/S transition is similarly inhibited, despite normal activation of the canonical ERK/MAPK pathway (Huang *et al.*, 1998). Cytoskeletal disruption also can prevent G1 progression in many cell types, including CE cells (Bohmer *et al.*, 1996; Ingber *et al.*, 1995; Iwig *et al.*, 1995; Reshetnikova *et al.*, 2000). Thus, additional signals that emanate from the intact cytoskeleton of spread cells in mid-G1 seem to be critical for the successful passage through late G1 and entry into S phase (Assoian, 1997; Huang and Ingber, 2002). Here, we describe how the techniques previously described can be used to analyze the molecular basis of cell shape–dependent control of cell cycle progression that characterizes virtually all normal anchorage-dependent cells.

Cell-cycle progression through the late G1/S restriction point, which represents the "point of no return" in the cell cycle, is associated with the hyperphosphorylation of retinoblastoma protein (pRb) by cyclin-dependent

kinases (cdks) (Assoian, 1997; Sherr and Roberts, 1999; Weinberg, 1995). Notably, the cdk inhibitor p27*kip1* (p27) that binds and inactivates the cyclin D1/cdk4 and cyclin E/cdk2 complexes is a major target for many physiologic growth regulatory signals (Pagano *et al.*, 1995). Importantly, when CE cell spreading is prevented by either altering the ECM substrate or disrupting the actin cytoskeleton with various cytoskeletal modulators, p27 levels remain high and cell-cycle progression is blocked in mid to late G1 (Huang *et al.*, 1998; Huang and Ingber, 2002; Mammoto *et al.*, 2004). The F-box protein Skp2 that is required for ubiquitination-dependent degradation of p27 restores G1 progression in these cells (Mammoto *et al.*, 2004). The effects of cell shape on cell-cycle progression are similarly mediated by p27 in other cell types (Carrano and Pagano, 2001; Zhu *et al.*, 1996). Thus, we measure phosphorylation level of pRb and the expression levels of Skp2 and p27 as markers for the G1/S transition. Any laboratory can use these quantitative methods, because they only require conventional molecular biologic and biochemical reagents, along with the ECM density modulation technique previously described; however, similar types of cell cycle analysis can be carried out with micropatterned ECM islands (Huang *et al.*, 1998).

5.1. Cell culture

Human microvascular endothelial (HMVE) cells from neonatal dermis and lung (Lonza) are cultured in EBM-2 (Lonza), supplemented with 5% fetal bovine serum (FBS) and growth factors (bFGF, insulin-like growth factor, vascular endothelial growth factor) according to the manufacturer's instructions and maintained at 37° in 5% CO_2 (Mammoto *et al.*, 2004). Cells are synchronized at the G0/G1 border by serum starvation (0.3% FBS/EBM-2) for 40 to 42 h and then released into G1 by trypsinizing the cells and replating them on ECM-coated (e.g., FN) bacteriologic dishes in EBM-2 containing 1% FBS and growth factors.

5.2. Cell-cycle analysis

We use various ways to detect G1/S transition, including BrdU incorporation and *in situ* labeling of pRb, as described previously, as well as the use of Western blotting and reverse transcription (RT)-PCR to detect cell cycle–associated proteins (Huang *et al.*, 1998; Mammoto *et al.*, 2004). For these latter forms of analysis, HMVE cells cultured on 60-mm dishes coated with various densities of FN (Ingber and Folkman, 1989b) are lysed with 0.3 ml of boiling lysis buffer (1% SDS, 50 mM Tris-HCl, pH 7.4), scraped, and lysates are collected at various time points after replating (4 to 24 h). Homogenized total cell lysates (10 μg protein) are subjected to SDS-PAGE, transferred to nitrocellulose membranes, and immunoblotted with

specific primary antibodies. The primary antibodies are detected with horseradish peroxidase–conjugated secondary antibodies (Vector Laboratories, Burlingame, CA) and Super Signal Ultra (Pierce) as a chemiluminescence substrate. Monoclonal antibody against pRb (LM95.1) is from Calbiochem (San Diego, CA), Skp2 (SKP2–8D9) is from Zymed Laboratories Inc. (San Francisco, CA), actin (AC-15) is from Sigma, and polyclonal antibody against p27 (clone 57) is purchased from Santa Cruz Biotechnologies (Santa Cruz, CA). Results are quantified by densitometric analysis with image J software.

RT-PCR is used to determine the expression of Skp2 mRNA. HMVE cells are lysed and total RNA was isolated with the RNeasy RNA extraction kit (Qiagen, Valencia, CA) according to instruction manual. The RNA (500 ng/sample) is treated for 1 h at 37° with reverse transcriptase with OMNI Script reverse-transcriptase assay kit (Qiagen). The PCR is carried out with a series of 1:3 dilutions of the RT product (2 μl). Only reactions in the log-linear range (product quantity versus input template quantity) are used. The forward and reverse PCR primers for Skp2 are 5′- CAAC TACCTCCAACACCTATC-3′ and 5′-TCCTGCCTATTTTCCCTGT TCT-3′, respectively. PCR cycling conditions are 3 min at 94°, then 26 cycles of 30 sec at 94°, 30 sec at 55°, and 1 min at 72°. For internal control, we use actin mRNA, whose forward and reverse primers are 5′-TGACGGGGTCACCCACACTGTGCC-3′ and 5′-TAGAAGCATT TGCGGTGGACGATG-3′, respectively. PCR products are analyzed by agarose gel electrophoresis. Primers are designed with Oligo version 4.0 software (National Biosciences, Plymouth, MN) and synthesized by Sigma Genosys (Biotechnologies Industries, The Woodlands, TX).

5.3. Determination of cell cycle position

To determine their position in the cell cycle, the levels of the critical G1 proteins, p27, Skp2, and pRb phosphorylation are measured in total cell lysates, with the phosphorylation status of pRb being used as a readout of successful progression through the late G1 restriction point. The point at which the levels of Skp2 and hyperphosphorylated pRb start to increase, and p27 begins to decrease, represents the G1 restriction point. This usually occurs between 12 and 18 h after replating synchronized CE cells on dishes coated with a high density (666 ng/cm^2) of FN that allows maximal cell spreading (Fig. 12.4). Round cells on a low density (22 ng/cm^2) of FN do not down-regulate p27, increase Skp2, or hyperphosphorylate pRb over the same time course, even though they are stimulated by the same soluble mitogens (bFGF, insulin-like growth factor, and vascular endothelial growth factor in 1% serum) (Fig. 12.4).

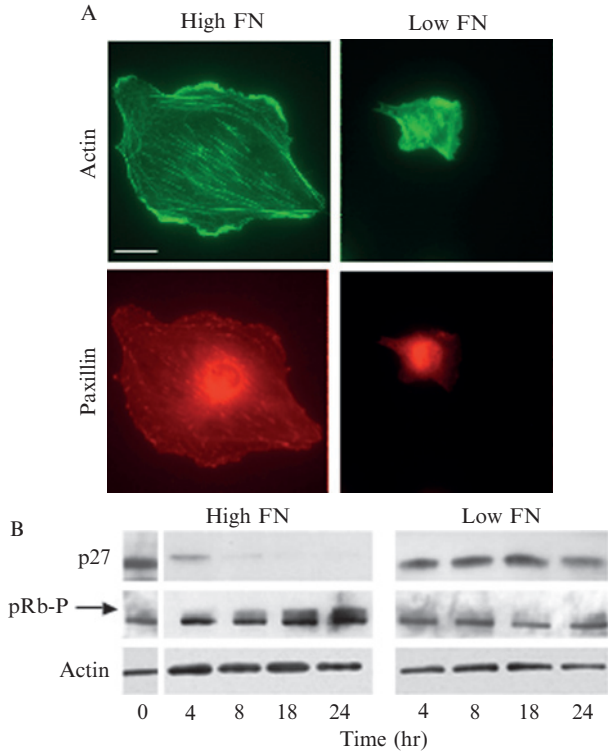

Figure 12.4 Variable ECM coating density method for analyzing cell shape–dependent control of cell cycle progression. (A) Fluorescence micrographs showing control of cell shape, stress fiber formation visualized with Alexa-488-phallodin and focal adhesion formation stained with anti-paxillin antibody in spread versus round HMVE cells on high versus low FN density (bar, 5 μm). Well-defined stress fibers and focal adhesions appear in highly spread cells on high FN, whereas round cells on low FN fail to exhibit either stress fibers or detectable focal adhesions. (B) Immunoblots showing changes in the level of expression of p27 protein relative to actin, as well as Rb protein phosphorylation status, in total cell lysates from spread and round cells cultured on high and low FN, respectively, for the indicated times after release from G0. For pRb, the slower-migrating (top) band represents the hyperphosphorylated form of the protein. The levels of hyperphosphorylated pRb increase and p27 decrease as the spread cells on high FN progress from G0 (time 0) to late G1 phase (from 8 to 18 h after release).

6. Methods for Analyzing Rho-Dependent Control of Cell Growth and Movement

The studies and methods previously described revealed that vascular cell growth, differentiation, and directional motility could vary greatly, depending on local variations in physical interactions between cells and

their ECM adhesions that alter cytoskeletal structure. Members of the Rho family of small GTPases, including Rho, Rac, and Cdc42, mediate the effects of cytokine and ECM binding on actin polymerization and cytoskeletal tension generation, which regulate stress fiber and focal adhesion assembly (Jaffe and Hall, 2005). However, recent findings show that physical changes in cytoskeletal structure produced by mechanical cues can also feed back to alter Rho activity (Mammoto *et al.*, 2004; 2007a). In fact, by use of protein transfection and FRET analysis techniques, we have found that Rho and Rac mediate cell shape–dependent control CE cell growth (Mammoto *et al.*, 2004) and directional lamellipodia formation (Brock and Ingber, 2005; Xia *et al.*, 2008). Thus, we present methods here that describe how control of cell growth and motility by Rho GTPases can be studied.

6.1. Preparation and delivery of recombinant Rho proteins

The constitutively active form of RhoA (RhoA14V) and the Rho activator, cytotoxic necrotizing factor 1 (CNF1), are expressed and purified from *Escherichia coli* expression plasmid pGEX4T-RhoA14V and pCNF24-CNF1 (kindly provided by Alan Hall, Memorial Sloan-Kettering Cancer Center, NY, and Melody Mills, Uniformed Services University of the Health Sciences, Bethesda, MD, respectively). GST-tagged RhoA14V and GST recombinant proteins are purified from *E. coli* (Mammoto *et al.*, 2004). For RhoA14V, the GST tag is removed by proteolytic cleavage with thrombin (10 units/ml, Sigma) at 4° for 8 to 10 h; thrombin is removed by incubating the supernatant with *p*-amino-benzamidine-agarose (Sigma). The His-tagged CNF1 is purified with Ni-agarose nitrilotriacetic acid beads following the manufacturer's instructions (Qiagen). C3 exoenzyme is purchased from Cytoskeleton Inc. (Denver, CO), and ROCK inhibitor Y27632 is purchased from Calbiochem.

For protein transfection (proteofection) of living cells, BioPORTER protein delivery reagent (Gene Therapy Systems, San Diego, CA) is used according to the manufacturer's instructions. In brief, 0.5 to 5 μg of recombinant protein in 200 μl of PBS is incubated in a tube containing a film of 15 μl of BioPORTER that is formed by drying for 5 min. The complexes are then added to the cells (400,000 cells/60-mm dish) in 2.5 ml of serum-free EBM-2; after 4 h of incubation at 37°, cells are replated onto the experimental FN-coated dishes with experimental medium. In the case of RhoA14V and C3, we use the BioPORTER reagent alone without added protein cargo as a proteofection control. CNF1 (100 ng/ml) and Y27632 (10 μM) are added to the medium when cells are replated. The samples are collected at the indicated time points after replating for cell cycle experiments and cell staining.

6.2. Rac FRET analysis

The small GTPase, Rac1, controls lamellipodia formation and cell motility, and it can be activated by cell–ECM adhesion in an integrin-dependent manner (Clark *et al.*, 1998; del Pozo *et al.*, 2000; Price *et al.*, 1998). An intramolecular Rac1-FRET reporter analysis allows us to characterize the spatial distribution of Rac activity in cells cultured on the different FN microarrays previously described. The FRET probe, Raichu-Rac1, was kindly provided by Dr. Michiyuki Matsuda (Osaka University, Osaka, Japan) (Itoh *et al.*, 2002). NIH 3T3 cells are transfected with the FRET reporter of Rac activity, Raichu-Rac1 with effectene transfection reagent (Qiagen, Valencia, CA), and cultured for 24 h on the different micropatterned substrates in serum-free medium. We studied cells cultured on the 3L-4.5,1 pattern (Fig. 12.3B) in studies analyzing spatial control of Rac activation dynamics at high resolution, because this pattern has the largest difference in island spacing between the X and Y directions. For FRET analysis, fluorescence images are acquired every minute on a Leica TCS SP2 confocal laser scanning microscope with a 63×/1.4 NA oil immersion objective with Leica FRET sensitization software (CFP and FRET excitation at 458 nm; YFP excitation at 514 nm). Calibration images are acquired from the samples containing only Donor (CFP), Acceptor (YFP) and FRET (Raichu-Rac1), respectively, and the software automatically calculates the apparent FRET efficiency.

7. Rho-Dependent Control of Angiogenesis in Whole Organ Culture

Tissue morphogenesis is controlled in embryonic tissues by altering the cellular mechanical force balance (Ingber, 2006; Moore *et al.*, 2005; Sanchez-Esteban *et al.*, 2006), and Rho-dependent control of cytoskeletal tension generation seems to play a central role in this process (Moore *et al.*, 2005). For example, when cytoskeletal tension generation is suppressed in whole lung organ rudiments cultured for 48 h after isolation from embryonic mice on day E12 with the Rho-associated kinase (ROCK) inhibitor Y27632 or other drugs (e.g., BDM, Cyto D or the MLCK inhibitor, ML-9) that inhibit cytoskeletal tension generation, epithelial budding is inhibited and the local thinning of the basement membrane that is normally observed in regions of new epithelial bud formation is lost (Fig. 12.5) (Moore *et al.*, 2005). By contrast, when cytoskeletal tension is increased by activating Rho with CNF-1, lung branching is accelerated. Importantly, increasing and decreasing cell tension, respectively, promotes and inhibits angiogenesis (capillary elongation) within the neighboring connective tissue (Fig. 12.5). Therefore, changes in cytoskeletal tension play an important role in the establishment of the regional variations in cell growth and ECM remodeling

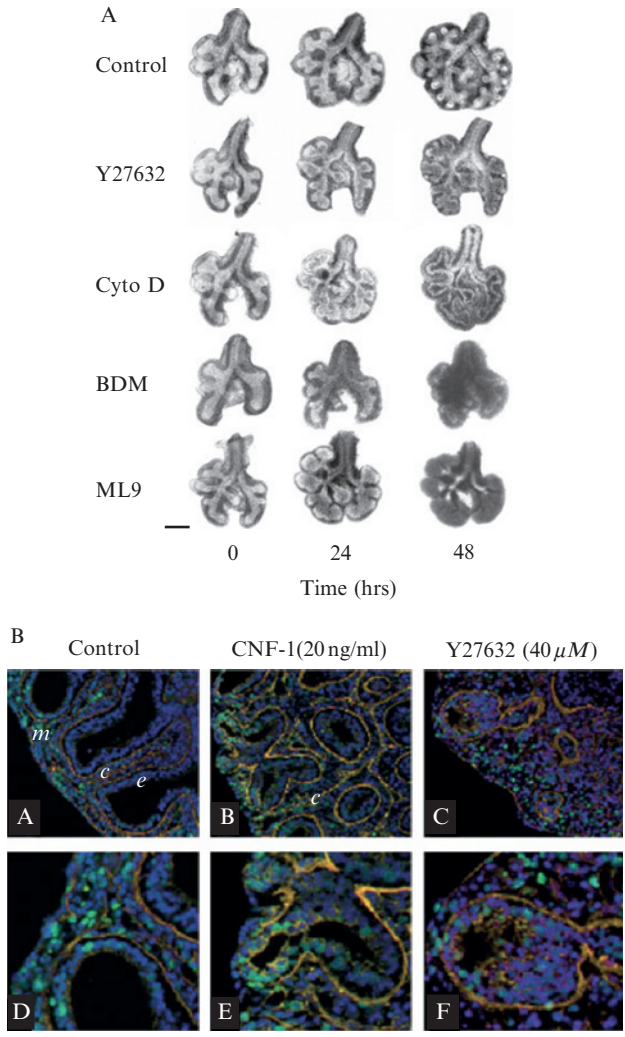

Figure 12.5 Rho-dependent control of lung epithelial and endothelial morphogenesis in whole embryonic organs. (A) Low-magnification bright-field views showing E12 mouse lung rudiment explants at time of isolation (time 0) and 24 and 48 h after treatment with agents that disrupt the cytoskeleton or suppress tension generation by various mechanisms. Lungs treated with Y27632 (40 μM) for 24 h or more exhibit enlarged bud ends and fail to form normal clefts or tight symmetric bud formation as seen in control lungs. Treatment with cyto D (100 ng/ml), BDM (20 mM), or ML9 (20 μM) completely prevents increases in epithelial bud number and size over a similar time course (scale bar, 500 μm). (B) Effects of the Rho stimulator CNF-1 and ROCK inhibitor Y27632 on epithelial and vascular development in developing lung rudiments. Immunofluorescence microscopic images of histologic sections through control lungs after 48 h culture in the absence (A and D) or presence of CNF-1 (20 ng/ml; B and E) or Y27632 (40 μM; C and F) and viewed at low (A to C) and high (D to F) magnification, showing BrdU

that drive epitheliogenesis and angiogenesis during embryonic organ development. In the developing lung, tensional forces exerted on capillary blood vessels, in part as a result of expansion of neighboring epithelial buds, apparently promote the elongation of these microvessels specifically in regions of lobular expansion.

7.1. Whole embryonic lung rudiment culture

Embryos from day 12 (E12) timed pregnant Swiss Webster mice (Taconic Farms, MA) are removed aseptically and placed into bacteriologic dishes containing Waymouth's MB medium (Invitrogen). Lung rudiments are microdissected en bloc (with all lobes still attached to the trachea), washed in serum-free medium, and transferred to a semipermeable membrane (Falcon cell inserts, 0.4-μm pore size) that is placed over 2.5 ml of serum-free BGJb medium (Fitton-Jackson modification; Invitrogen) supplemented with penicillin, streptomycin, and ascorbic acid (0.2 mg/ml) in a 6-well plate. Three lungs are placed in each well and subjected to the same dose of pharmacologic agent, which is added to individual wells at 0 h and again at 24 h with fresh BGJb medium. The agents included cyto D (100 ng/ml; Sigma), BDM (20 m*M*; Sigma), ML9 (20 μM; Sigma), Y27632 (10, 20, or 40 μM; Calbiochem), or CNF-1 (2, 20, or 200 ng/ml). *In vitro* development is monitored within whole organs by morphologic observations and serial measurements of branch points (number of buds) at 12-h intervals from 0 to 48 h with light microscopy. Results are expressed as percentage increase in number of terminal lung buds formed at each branch point relative to Time 0 baseline controls ($n = 9$ lungs/condition). Data are analyzed with an analysis of variance (ANOVA) single factor test and the two-sample independent *t* test.

incorporation (green), laminin (red), and DAPI-stained nuclei (blue). Note that control lung contains the greatest number of growing cells along the periphery of the growing epithelium in regions where the basement membrane thins. Well-developed capillaries (*c*) surrounded by their own basement membrane can been seen within the mesenchyme (*m*) between adjacent epithelial buds (*e*). Also, treatment with CNF-1 at 20 ng/ml results in increased numbers of epithelial buds and cell proliferation, although the proliferating cells remain localized to the periphery of the gland near regions of basement membrane thinning. CNF-1 treatment also promotes further extension and elongation of these capillary networks (*c*) in parallel with extension of the epithelium. In contrast, treatment with Y27632 inhibits basement membrane thinning and results in piled up clusters of disorganized cells that fill much of the epithelial lumen. Proliferative cells are still detected; however, their normal spatial localization at the periphery is lost. ROCK inhibition also results in disorganization of vascular architecture and disruption of the capillary network formation, because CE cells appear to be bunched together within isolated cell clusters.

7.2. Quantification of cell proliferation *in vivo*

Cell proliferation in lung rudiments is measured by quantifying the percentage of cells that exhibited nuclear incorporation of BrdU in control and drug-treated lungs that are pulsed with BrdU (10 μM, Amersham, Arlington Heights, IL) from hours 42 to 48 in culture. Lungs are fixed in 4% PFA for 1 h at room temperature, dehydrated, and paraffin-embedded. Three micrometer-thick sections are cut, deparaffinized, rehydrated, treated with proteinase K (10 μg/ml; Sigma) for 20 min at room temperature, blocked in TNB buffer (NEL-700A, NEN Life Sciences Products, Boston, MA), probed with a monoclonal mouse antibody against BrdU (RPN-202, Amersham) for 90 min at room temperature, detected with a biotinylated goat anti-mouse IgG antibody (BA-9200, Vector) and Texas Red–avidin (A2006, Vector), and counterstained with Hoescht (1:1,000). BrdU-positive fluorescent cells are visualized and scored with a Nikon Diaphot microscope with 25 and 63 objectives and the IPLab image acquisition and processing computer program (Vaytek). At least five random fields are counted per sample. Results are presented as percentage of cells incorporating BrdU. Data are analyzed by use of an ANOVA single-factor test and the two-sample independent *t* test.

7.3. Immunohistochemistry

Lungs are fixed in 4% PFA, paraffin-embedded, sectioned (3 μm), and stained with hematoxylin and eosin for light microscopic analysis. To visualize laminin in basement membrane, paraffin sections are treated with proteinase K (10 μg/ml) for 20 min at room temperature, blocked in TNB buffer, probed with a rabbit polyclonal anti-laminin antibody (L9393, Sigma; 1:100), detected by use of a biotinylated goat anti-rabbit antibody (BA-1000, Vector; 1:400) and Texas Red avidin (A2006, Vector; 1:250), counterstained with Hoechst (1:1,000), and visualized by use of immunofluorescence microscopy. Actin is visualized in the cytoskeleton of cells with a fluorescein isothiocyanate–conjugated monoclonal anti-actin antibody (F3046, Sigma, 1:50) in parallel sections.

8. Rho-Dependent Control of Vascular Permeability

In addition to regulating angiogenesis, Rho and Rac are also central modulators of vascular permeability (Birukova *et al.*, 2004; Mammoto *et al.*, 2007b; Wojciak-Stothard *et al.*, 2001). We recently showed that the Rho inhibitor, p190RhoGAP, mediates the vessel sealing effects of angiopoietin-1 (Ang-1) by balancing Rho and Rac activities (Mammoto *et al.*, 2007b).

Given that p190RhoGAP mediates cytoskeleton-dependent inactivation of Rho (Mammoto *et al.*, 2007a), resulting changes in the cytoskeleton may also feed back to further modulate Rho and its vessel sealing effects. In any case, completion of these studies required lentiviral transduction of Rho proteins into CE cells and *in vivo* delivery of siRNA into vascular endothelial cells. Thus, we describe these methods here because they may be useful to other investigators as well.

8.1. Lentiviral transduction of Rho proteins

The dominant negative form of Rac1 (Rac1T17N) and the constitutively active form of RhoA (RhoAG14V) are constructed by PCR with pcDNA-Rac1T17N or -RhoAG14V (University of Missouri, Rolla, cDNA Resource Center) as a template and subcloned into the pHAGE lentiviral backbone vector at the *NotI/BamHI* sites. Generation of lentiviral vectors is accomplished by a five-plasmid transfection procedure (Mostoslavsky *et al.*, 2005). 293T cells are transfected with TransIT 293 (Mirus, Madison, WI) according to the manufacturer's instructions with the backbone pHAGE vector together with four expression vectors encoding the packaging proteins Gag-pol, Rev, Tat, and the G protein of the vesicular stomatitis virus (VSV). Viral supernatants are collected starting 48 h after transfection, for four consecutive times every 12 h, pooled, and filtered through a 0.45-μm filter. Viral supernatants are then concentrated 100-fold by ultracentrifugation in a Beckman centrifuge, for 1.5 h at 16,500 rpm. By use of these protocols, titers of 5×10^8 to 1×10^9/ml are achieved. HMVE cells are incubated with viral stocks in the presence of 5 μg/ml polybrene (sigma) and 90 to 100% infection is achieved 3 days later (Mammoto *et al.*, 2007b).

8.2. *In vitro* transendothelial permeability assays

HMVE cells from lung (1×10^5 cells in 100 μl of the medium) are seeded onto Coster Transwell membranes (6.5-mm diameter, 0.4-μm pore size) coated with 1% gelatin or fibronectin. After 1-day incubation (the cells reach confluent), the abluminal and luminal medium is carefully aspirated and replaced with the medium (100 μl medium supplemented with FITC-dextran at the final concentration of 1 mg/ml for luminal chamber and 600 μl medium for abluminal chamber). At the desired time points, samples are taken from both the luminal and abluminal chamber for fluorometry analysis (λex 485 nm; λem 525 nm). The readings are converted with the use of a standard curve to albumin concentration. These concentrations are then used in the following equation to determine the permeability coefficient of albumin (Pa): $Pa = [A]/t \times 1/A \times V/[L]$, ([A]; abluminal concentration, where t is time in seconds, A is the area of membrane in cm^2, V is the

volume of abluminal chamber, and *[L]* is the luminal concentration). Data are analyzed from a representative of at least three experiments.

8.3. *In vivo* vascular permeability assay

FVB mice (6- to 8-weeks of age) are anesthetized with intraperitoneal Avertin (2,2,2 Tribromoethanol) (125 to 240 mg/kg). 2% Evans blue (50 μl) is then injected into the retroorbital sinus or tail vein. Ten minutes after the Evans blue injection, mice are sacrificed and perfused with PBS with 2 m*M* EDTA for 10 min through a canula placed in the right ventricle. Blood and PBS are vented through an incision in the vena cava, thus allowing perfusate to pass through the pulmonary and systemic circulations. After 10 min of perfusion, the outflow from the vena cava is observed to be clear, confirming that blood (and intravascular Evans blue) had been flushed out the circulation. Organs (e.g., lungs, liver) are then harvested and homogenized in 1.5 ml of formamide. Evans blue is eluted by incubating the samples at 70° for 24 h, and the concentration of Evans blue is estimated by dual-wavelength spectrophotometer (620 nm and 740 nm). The following formula is used to correct optical densities (E) for contamination with heme pigments: E620 (corrected) = E620 (raw) − (1.426 × E740 (raw) + 0.03).

In vivo delivery of siRNA is used to knock down the gene. Delivery of siRNA into mice is performed with TransIT hydrodynamic delivery solution (Mirus, Madison, WI) according to the manufacturer's instructions. Mice are injected with either 10 μg of control siRNA or interested-gene siRNA in 1 ml of delivery solution into the tail vein over 7 sec. The method of siRNA delivery is known to suppress 80 to 90% gene expression in multiple organs, including the lung (Mammoto *et al.*, 2007b). High-pressure hydrodynamic delivery does not adversely affect serum chemistries or result in end-organ injury (Liu *et al.*, 1999). Three days after injection, a lung permeability assay is performed. Gene knockdown is confirmed by lysing organs in RIPA buffer and immunoblotting with specific antibody. Mouse lung wet-to-dry weight ratio (W/D ratio) is used to measure lung water accumulation. Lung wet weight is determined immediately after removal of the lung. Lung dry weight is determined after the lung is dried in an oven at 50° for 24 h. The W/D ratio is calculated by dividing the wet weight by the dry weight.

9. Conclusion

Vascular cell behavior is controlled through interplay between mechanical and chemical stimuli that regulate intracellular biochemistry. Understanding the molecular biophysical basis of mechanotransduction,

therefore, represents a critically important challenge in vascular biology. As described in this chapter, we have developed various hybrid techniques that combine approaches from materials science and engineering with more conventional cell and molecular biologic tools to meet this challenge. These methods may be used to help better understand the fundamental mechanisms that underlie vascular control. In the future, these techniques may be further modified for more extensive use *in vivo*, which may greatly facilitate development of novel therapeutic approaches for various angiogenesis-dependent diseases, including cancer, arthritis, and various forms of blindness.

ACKNOWLEDGMENTS

This work was supported by grants from NIH, NASA, DARPA ,and DoD; D. E. I. is also a recipient of a DoD Breast Cancer Innovator Award.

REFERENCES

Amiji, M., and Park, K. (1992). Prevention of protein adsorption and platelet adhesion on surfaces by PEO/PPO/PEO triblock copolymers. *Biomaterials* **13,** 682–962.

Assoian, R. K. (1997). Anchorage-dependent cell cycle progression. *J. Cell Biol.* **136,** 1–4.

Beningo, K. A., Dembo, M., Kaverina, I., Small, J. V., and Wang, Y. L. (2001). Nascent focal adhesions are responsible for the generation of strong propulsive forces in migrating fibroblasts. *J. Cell Biol.* **153,** 881–888.

Bhatia, S. K., Teixeira, J. L., Anderson, M., Shriver-Lake, L. C., Calvert, J. M., Georger, J. H., Hickman, J. J., Dulcey, C. S., Schoen, P. E., and Ligler, F. S. (1993). Fabrication of surfaces resistant to protein adsorption and application to two-dimensional protein patterning. *Anal. Biochem.* **208,** 197–205.

Birukova, A. A., Smurova, K., Birukov, K. G., Kaibuchi, K., Garcia, J. G., and Verin, A. D. (2004). Role of Rho GTPases in thrombin-induced lung vascular endothelial cells barrier dysfunction. *Microvasc. Res.* **67,** 64–77.

Blanchard, E. M., Smith, G. L., Allen, D. G., and Alpert, N. R. (1990). The effects of 2,3-butanedione monoxime on initial heat, tension, and aequorin light output of ferret papillary muscles. *Pflüger's Arch.* **416,** 219–221.

Bohmer, R. M., Scharf, E., and Assoian, R. K. (1996). Cytoskeletal integrity is required throughout the mitogen stimulation phase of the cell cycle and mediates the anchorage-dependent expression of cyclin D1. *Mol. Biol. Cell* **7,** 101–111.

Brock, A., Chang, E., Ho, C. C., LeDuc, P., Jiang, X., Whitesides, G. M., and Ingber, D. E. (2003). Geometric determinants of directional cell motility revealed using microcontact printing. *Langmuir* **19,** 1611–1617.

Brock, A. L., and Ingber, D. E. (2005). Control of the direction of lamellipodia extension through changes in the balance between Rac and Rho activities. *Mol. Cell Biomech.* **2,** 135–143.

Carrano, A. C., and Pagano, M. (2001). Role of the F-box protein Skp2 in adhesion-dependent cell cycle progression. *J. Cell Biol.* **153,** 1381–1390.

Casciola-Rosen, L. A., Miller, D. K., Anhalt, G. J., and Rosen, A. (1994). Specific cleavage of the 70-kDa protein component of the U1 small nuclear ribonucleoprotein is a

characteristic biochemical feature of apoptotic cell death. *J. Biol. Chem.* **269,** 30757–30760.
Chalovich, J. M., Sen, A., Resetar, A., Leinweber, B., Fredricksen, R. S., Lu, F., and Chen, Y. D. (1998). Caldesmon: Binding to actin and myosin and effects on elementary steps in the ATPase cycle. *Acta Physiol. Scand.* **164,** 427–435.
Chen, C. S., Alonso, J. L., Ostuni, E., Whitesides, G. M., and Ingber, D. E. (2003). Cell shape provides global control of focal adhesion assembly. *Biochem. Biophys. Res. Commun.* **307,** 355–361.
Chen, C. S., Mrksich, M., Huang, S., Whitesides, G. M., and Ingber, D. E. (1997). Geometric control of cell life and death. *Science* **276,** 1425–1428.
Chen, C. S., Ostuni, E., Whitesides, G. M., and Ingber, D. E. (2000). Using self-assembled monolayers to pattern ECM proteins and cells on substrates. *Methods Mol. Biol.* **139,** 209–219.
Chen, C. S., Tan, J., and Tien, J. (2004). Mechanotransduction at cell-matrix and cell-cell contacts. *Annu. Rev. Biomed. Eng.* **6,** 275–302.
Chicurel, M. E., Singer, R. H., Meyer, C. J., and Ingber, D. E. (1998). Integrin binding and mechanical tension induce movement of mRNA and ribosomes to focal adhesions. *Nature* **392,** 730–733.
Chrzanowska-Wodnicka, M., and Burridge, K. (1996). Rho-stimulated contractility drives the formation of stress fibers and focal adhesions. *J. Cell Biol.* **133,** 1403–1415.
Clark, E. A., King, W. G., Brugge, J. S., Symons, M., and Hynes, R. O. (1998). Integrin-mediated signals regulated by members of the rho family of GTPases. *J. Cell Biol.* **142,** 573–586.
del Pozo, M. A., Price, L. S., Alderson, N. B., Ren, X. D., and Schwartz, M. A. (2000). Adhesion to the extracellular matrix regulates the coupling of the small GTPase Rac to its effector PAK. *EMBO J.* **19,** 2008–2014.
Dike, L. E., Chen, C. S., Mrksich, M., Tien, J., Whitesides, G. M., and Ingber, D. E. (1999). Geometric control of switching between growth, apoptosis, and differentiation during angiogenesis using micropatterned substrates. *In Vitro Cell Dev. Biol. Anim.* **35,** 441–448.
Discher, D. E., Janmey, P., and Wang, Y. L. (2005). Tissue cells feel and respond to the stiffness of their substrate. *Science* **310,** 1139–1143.
Flusberg, D. A., Numaguchi, Y., and Ingber, D. E. (2001). Cooperative control of Akt phosphorylation, bcl-2 expression, and apoptosis by cytoskeletal microfilaments and microtubules in capillary endothelial cells. *Mol. Biol. Cell* **12,** 3087–3094.
Folkman, J., Haudenschild, C. C., and Zetter, B. R. (1979). Long-term culture of capillary endothelial cells. *Proc. Natl. Acad. Sci. USA* **76,** 5217–5221.
Folkman, J., Watson, K., Ingber, D., and Hanahan, D. (1989). Induction of angiogenesis during the transition from hyperplasia to neoplasia. *Nature* **339,** 58–61.
Gray, D. S., Tien, J., and Chen, C. S. (2003). Repositioning of cells by mechanotaxis on surfaces with micropatterned Young's modulus. *J. Biomed. Mater. Res. A* **66,** 605–614.
Helfman, D. M., Levy, E. T., Berthier, C., Shtutman, M., Riveline, D., Grosheva, I., Lachish-Zalait, A., Elbaum, M., and Bershadsky, A. D. (1999). Caldesmon inhibits nonmuscle cell contractility and interferes with the formation of focal adhesions. *Mol. Biol. Cell* **10,** 3097–3112.
Huang, S., Chen, C. S., and Ingber, D. E. (1998). Control of cyclin D1, p27(Kip1), and cell cycle progression in human capillary endothelial cells by cell shape and cytoskeletal tension. *Mol. Biol. Cell* **9,** 3179–3193.
Huang, S., and Ingber, D. E. (1999). The structural and mechanical complexity of cell-growth control. *Nat. Cell Biol.* **1,** E131–E138.
Huang, S., and Ingber, D. E. (2002). A discrete cell cycle checkpoint in late G(1) that is cytoskeleton-dependent and MAP kinase (Erk)–independent. *Exp. Cell Res.* **275,** 255–264.

Huber, P. A. (1997). Caldesmon. *Int. J. Biochem. Cell Biol.* **29,** 1047–1051.
Ingber, D. E. (1990). Fibronectin controls capillary endothelial cell growth by modulating cell shape. *Proc. Natl. Acad. Sci. USA* **87,** 3579–3583.
Ingber, D. E. (2006). Mechanical control of tissue morphogenesis during embryological development. *Int. J. Dev. Biol.* **50,** 255–266.
Ingber, D. E., and Folkman, J. (1989a). How does extracellular matrix control capillary morphogenesis? *Cell* **58,** 803–805.
Ingber, D. E., and Folkman, J. (1989b). Mechanochemical switching between growth and differentiation during fibroblast growth factor–stimulated angiogenesis *in vitro*: Role of extracellular matrix. *J. Cell Biol.* **109,** 317–330.
Ingber, D. E., Madri, J. A., and Folkman, J. (1987). Endothelial growth factors and extracellular matrix regulate DNA synthesis through modulation of cell and nuclear expansion. *In Vitro Cell Dev. Biol.* **23,** 387–394.
Ingber, D. E., Madri, J. A., and Jamieson, J. D. (1985). Neoplastic disorganization of pancreatic epithelial cell–cell relations. Role of basement membrane. *Am. J. Pathol.* **121,** 248–260.
Ingber, D. E., Prusty, D., Sun, Z., Betensky, H., and Wang, N. (1995). Cell shape, cytoskeletal mechanics, and cell cycle control in angiogenesis. *J. Biomech.* **28,** 1471–1484.
Itoh, R. E., Kurokawa, K., Ohba, Y., Yoshizaki, H., Mochizuki, N., and Matsuda, M. (2002). Activation of rac and cdc42 video imaged by fluorescent resonance energy transfer–based single-molecule probes in the membrane of living cells. *Mol. Cell Biol.* **22,** 6582–6591.
Iwig, M., Czeslick, E., Muller, A., Gruner, M., Spindler, M., and Glaesser, D. (1995). Growth regulation by cell shape alteration and organization of the cytoskeleton. *Eur. J. Cell Biol.* **67,** 145–157.
Jaffe, A. B., and Hall, A. (2005). Rho GTPases: Biochemistry and biology. *Annu. Rev. Cell Dev. Biol.* **21,** 247–269.
Kim, B. S., Nikolovski, J., Bonadio, J., Smiley, E., and Mooney, D. J. (1999). Engineered smooth muscle tissues: Regulating cell phenotype with the scaffold. *Exp. Cell Res.* **251,** 318–328.
Kim, B. S., Putnam, A. J., Kulik, T. J., and Mooney, D. J. (1998). Optimizing seeding and culture methods to engineer smooth muscle tissue on biodegradable polymer matrices. *Biotechnol. Bioeng.* **57,** 46–54.
Kumar, A., and Whitesides, G. M. (1994). Patterned condensation figures as optical diffraction gratings. *Science* **263,** 60–62.
Latham, K. M., Eastman, S. W., Wong, A., and Hinds, P. W. (1996). Inhibition of p53-mediated growth arrest by overexpression of cyclin-dependent kinases. *Mol. Cell Biol.* **16,** 4445–4455.
Lazebnik, Y. A., Kaufmann, S. H., Desnoyers, S., Poirier, G. G., and Earnshaw, W. C. (1994). Cleavage of poly(ADP-ribose) polymerase by a proteinase with properties like ICE. *Nature* **371,** 346–347.
Lee, K. M., Tsai, K. Y., Wang, N., and Ingber, D. E. (1998). Extracellular matrix and pulmonary hypertension: Control of vascular smooth muscle cell contractility. *Am. J. Physiol.* **274,** H76–H82.
Lele, T. P., Sero, J. E., Matthews, B. D., Kumar, S., Xia, S., Montoya-Zavala, M., Polte, T., Overby, D., Wang, N., and Ingber, D. E. (2007). Tools to study cell mechanics and mechanotransduction. *Methods Cell Biol.* **83,** 443–472.
Li, P., Nijhawan, D., Budihardjo, I., Srinivasula, S. M., Ahmad, M., Alnemri, E. S., and Wang, X. (1997). Cytochrome c and dATP-dependent formation of Apaf-1/caspase-9 complex initiates an apoptotic protease cascade. *Cell* **91,** 479–489.
Liu, F., Song, Y., and Liu, D. (1999). Hydrodynamics-based transfection in animals by systemic administration of plasmid DNA. *Gene Ther.* **6,** 1258–1266.

Lo, C. M., Wang, H. B., Dembo, M., and Wang, Y. L. (2000). Cell movement is guided by the rigidity of the substrate. *Biophys. J.* **79,** 144–152.

Mammoto, A., Huang, S., and Ingber, D. E. (2007a). Filamin links cell shape and cytoskeletal structure to Rho regulation by controlling accumulation of p190RhoGAP in lipid rafts. *J. Cell Sci.* **120,** 456–467.

Mammoto, A., Huang, S., Moore, K., Oh, P., and Ingber, D. E. (2004). Role of RhoA, mDia, and ROCK in cell shape–dependent control of the Skp2-p27kip1 pathway and the G1/S transition. *J. Biol. Chem.* **279,** 26323–26330.

Mammoto, T., Parikh, S. M., Mammoto, A., Gallagher, D., Chan, B., Mostoslavsky, G., Ingber, D. E., and Sukhatme, V. P. (2007). Angiopoietin-1 requires p190RhoGAP to protect against vascular leakage *in vivo*. *J. Biol. Chem* **282,** 23910–23918.

Marston, S. B., Fraser, I. D., and Huber, P. A. (1994). Smooth muscle caldesmon controls the strong binding interaction between actin-tropomyosin and myosin. *J. Biol. Chem.* **269,** 32104–32109.

Matsumoto, T., Yung, Y. C., Fischbach, C., Kong, H. J., Nakaoka, R., and Mooney, D. J. (2007). Mechanical strain regulates endothelial cell patterning *in vitro*. *Tissue Eng.* **13,** 207–217.

Matsumura, F., and Yamashiro, S. (1993). Caldesmon. *Curr. Opin. Cell Biol.* **5,** 70–76.

Matthews, B. D., Overby, D. R., Mannix, R., and Ingber, D. E. (2006). Cellular adaptation to mechanical stress: Role of integrins, Rho, cytoskeletal tension and mechanosensitive ion channels. *J. Cell Sci.* **119,** 508–518.

Meloche, S., Pages, G., and Pouyssegur, J. (1992). Functional expression and growth factor activation of an epitope-tagged p44 mitogen-activated protein kinase, p44mapk. *Mol. Biol. Cell* **3,** 63–71.

Mittnacht, S., and Weinberg, R. A. (1991). G1/S phosphorylation of the retinoblastoma protein is associated with an altered affinity for the nuclear compartment. *Cell* **65,** 381–393.

Mooney, D., Hansen, L., Vacanti, J., Langer, R., Farmer, S., and Ingber, D. (1992). Switching from differentiation to growth in hepatocytes: Control by extracellular matrix. *J. Cell Physiol.* **151,** 497–505.

Moore, K. A., Polte, T., Huang, S., Shi, B., Alsberg, E., Sunday, M. E., and Ingber, D. E. (2005). Control of basement membrane remodeling and epithelial branching morphogenesis in embryonic lung by Rho and cytoskeletal tension. *Dev. Dyn.* **232,** 268–281.

Mostoslavsky, G., Kotton, D. N., Fabian, A. J., Gray, J. T., Lee, J. S., and Mulligan, R. C. (2005). Efficiency of transduction of highly purified murine hematopoietic stem cells by lentiviral and oncoretroviral vectors under conditions of minimal *in vitro* manipulation. *Mol. Ther.* **11,** 932–940.

Muzio, M., Salvesen, G. S., and Dixit, V. M. (1997). FLICE induced apoptosis in a cell-free system. Cleavage of caspase zymogens. *J. Biol. Chem.* **272,** 2952–2956.

Nakatsuji, N., and Johnson, K. E. (1984). Experimental manipulation of a contact guidance system in amphibian gastrulation by mechanical tension. *Nature* **307,** 453–455.

Numaguchi, Y., Huang, S., Polte, T. R., Eichler, G. S., Wang, N., and Ingber, D. E. (2003). Caldesmon-dependent switching between capillary endothelial cell growth and apoptosis through modulation of cell shape and contractility. *Angiogenesis* **6,** 55–64.

Pagano, M., Tam, S. W., Theodoras, A. M., Beer-Romero, P., Del Sal, G., Chau, V., Yew, P. R., Draetta, G. F., and Rolfe, M. (1995). Role of the ubiquitin-proteasome pathway in regulating abundance of the cyclin-dependent kinase inhibitor p27. *Science* **269,** 682–685.

Parker, K. K., Brock, A. L., Brangwynne, C., Mannix, R. J., Wang, N., Ostuni, E., Geisse, N. A., Adams, J. C., Whitesides, G. M., and Ingber, D. E. (2002). Directional control of lamellipodia extension by constraining cell shape and orienting cell tractional forces. *FASEB J.* **16,** 1195–1204.

Pelham, R. J., and Wang, Y. (1997). Cell locomotion and focal adhesions are regulated by substrate flexibility. *Proc. Natl. Acad. Sci. USA* **94,** 13661–13665.

Pietramaggiori, G., Liu, P., Scherer, S. S., Kaipainen, A., Prsa, M. J., Mayer, H., Newalder, J., Alperovich, M., Mentzer, S. J., Konerding, M. A., Huang, S., Ingber, D. E., and Orgill, D. P. (2007). Tensile forces stimulate vascular remodeling and epidermal cell proliferation in living skin. *Ann. Surg.* **246,** 896–902.

Price, L. S., Leng, J., Schwartz, M. A., and Bokoch, G. M. (1998). Activation of Rac and Cdc42 by integrins mediates cell spreading. *Mol. Biol. Cell* **9,** 1863–1871.

Prime, K., and Whitesides, G. (1991). Self-assembled organic monolayers: Model systems for studying adsorption of proteins at surfaces. *Science* **252,** 1164–1167.

Reshetnikova, G., Barkan, R., Popov, B., Nikolsky, N., and Chang, L. S. (2000). Disruption of the actin cytoskeleton leads to inhibition of mitogen-induced cyclin E expression, Cdk2 phosphorylation, and nuclear accumulation of the retinoblastoma protein-related p107 protein. *Exp. Cell Res.* **259,** 35–53.

Ridley, A. J., Schwartz, M. A., Burridge, K., Firtel, R. A., Ginsberg, M. H., Borisy, G., Parsons, J. T., and Horwitz, A. R. (2003). Cell migration: Integrating signals from front to back. *Science* **302,** 1704–1709.

Riveline, D., Zamir, E., Balaban, N. Q., Schwarz, U. S., Ishizaki, T., Narumiya, S., Kam, Z., Geiger, B., and Bershadsky, A. D. (2001). Focal contacts as mechanosensors: Externally applied local mechanical force induces growth of focal contacts by an mDia1-dependent and ROCK-independent mechanism. *J. Cell Biol.* **153,** 1175–1186.

Sanchez-Esteban, J., Wang, Y., Filardo, E. J., Rubin, L. P., and Ingber, D. E. (2006). Integrins beta1, alpha6, and alpha3 contribute to mechanical strain-induced differentiation of fetal lung type II epithelial cells via distinct mechanisms. *Am. J. Physiol. Lung Cell Mol. Physiol.* **290,** L343–L350.

Schwartz, M. A., Lechene, C., and Ingber, D. E. (1991). Insoluble fibronectin activates the Na/H antiporter by clustering and immobilizing integrin alpha 5 beta 1, independent of cell shape. *Proc. Natl. Acad. Sci. USA* **88,** 7849–7853.

Sherr, C. J., and Roberts, J. M. (1999). CDK inhibitors: Positive and negative regulators of G1-phase progression. *Genes Dev.* **13,** 1501–1512.

Singhvi, R., Kumar, A., Lopez, G. P., Stephanopoulos, G. N., Wang, D. I., Whitesides, G. M., and Ingber, D. E. (1994). Engineering cell shape and function. *Science* **264,** 696–698.

Srinivasula, S. M., Ahmad, M., Fernandes-Alnemri, T., Litwack, G., and Alnemri, E. S. (1996). Molecular ordering of the Fas-apoptotic pathway: The Fas/APO-1 protease Mch5 is a CrmA-inhibitable protease that activates multiple Ced-3/ICE-like cysteine proteases. *Proc. Natl. Acad. Sci. USA* **93,** 14486–14491.

Tan, J. L., Tien, J., and Chen, C. S. (2002). Microcontact printing of proteins on mixed self-assembled monolayers. *Langmuir* **18,** 519–523.

Tan, J. L., Tien, J., Pirone, D. M., Gray, D. S., Bhadriraju, K., and Chen, C. S. (2003). Cells lying on a bed of microneedles: An approach to isolate mechanical force. *Proc. Natl. Acad Sci. USA* **100,** 1484–1489.

Thakar, R. G., Ho, F., Huang, N. F., Liepmann, D., and Li, S. (2003). Regulation of vascular smooth muscle cells by micropatterning. *Biochem. Biophys. Res. Commun.* **307,** 883–890.

Tzima, E. (2006). Role of small GTPases in endothelial cytoskeletal dynamics and the shear stress response. *Circ. Res.* **98,** 176–185.

Van Haastert, P. J., and Devreotes, P. N. (2004). Chemotaxis: Signalling the way forward. *Nat. Rev. Mol. Cell Biol.* **5,** 626–634.

Wang, N., Butler, J. P., and Ingber, D. E. (1993). Mechanotransduction across the cell surface and through the cytoskeleton. *Science* **260,** 1124–1127.

Weber, J. D., Raben, D. M., Phillips, P. J., and Baldassare, J. J. (1997). Sustained activation of extracellular-signal-regulated kinase 1 (ERK1) is required for the continued expression of cyclin D1 in G1 phase. *Biochem. J.* **326**(Pt 1), 61–68.

Weinberg, R. A. (1995). The retinoblastoma protein and cell cycle control. *Cell* **81,** 323–330.

Whitesides, G. M., Ostuni, E., Takayama, S., Jiang, X., and Ingber, D. E. (2001). Soft lithography in biology and biochemistry. *Annu. Rev. Biomed. Eng.* **3,** 335–373.

Wojciak-Stothard, B., Potempa, S., Eichholtz, T., and Ridley, A. J. (2001). Rho and Rac but not Cdc42 regulate endothelial cell permeability. *J. Cell Sci.* **114,** 1343–1355.

Xia, N., Thodeti, C. K., Hunt T. P., Xu Q., Ho, M., Whitesides, G. M., Westervelt, R., Ingber, D. E. (2008) Directional control of cell motility through focal adhesion positioning and spatial control of Rac activation. *FASEB J.* **22,** 1649–1659.

Yu, J., Moon, A., and Kim, H. R. (2001). Both platelet-derived growth factor receptor (PDGFR)-alpha and PDGFR-beta promote murine fibroblast cell migration. *Biochem. Biophys. Res. Commun.* **282,** 697–700.

Zhu, X., and Assoian, R. K. (1995). Integrin-dependent activation of MAP kinase: A link to shape-dependent cell proliferation. *Mol. Biol. Cell* **6,** 273–282.

Zhu, X., Ohtsubo, M., Bohmer, R. M., Roberts, J. M., and Assoian, R. K. (1996). Adhesion-dependent cell cycle progression linked to the expression of cyclin D1, activation of cyclin E-cdk2, and phosphorylation of the retinoblastoma protein. *J. Cell Biol.* **133,** 391–403.